Insight into Global Reaction Mechanism of [C_2, H_4, O] System from ab Initio Calculations by the Scaled Hypersphere Search Method

Xia Yang, Satoshi Maeda, and Koichi Ohno*

Department of Chemistry, Graduate School of Science, Tohoku University, Aramaki, Aoba-ku, Sendai 980-8578, Japan

Received: February 13, 2007; In Final Form: April 2, 2007

A detailed computational study is performed on the singlet potential energy surface (PES) for possible isomerization and dissociation reactions of CH_3CHO at the DFT (B3LYP/6-311++G(d,p)) and CCSD(T)/cc-pVTZ//B3LYP/6-311++G(d,p) levels. The pathways around the equilibrium structures can be discovered by the scaled hypersphere search (SHS) method, which enables us to make a global analysis of the PES for a given chemical composition. Fourteen isomers inclusive of 11 single-molecules and three "non-stabilized" oxygen-based ylides, 5 energetically favored complexes, and 79 interconversion transition states have been found on the singlet PES. Four lowest lying isomers with thermodynamic stability are also kinetically stable with respect to metastable intermediates. It was revealed that vinyl alcohols, which could be generated by the tautomerization of acetaldehyde, could undergo dissociation to form acetylene and water. In addition, recombination channels between some fragments, such as $H_2CO + {}^1CH_2$ and $^1CHOH + {}^1CH_2$, are energetically accessible via collision complex or oxygen-based ylides. Most of available unimolecular decompositions are found to be responsible for favorable hydrogen abstraction processes.

1. Introduction

Acetaldehyde, a typical aldehyde molecule of [C_2, H_4, O] system, is among the key intermediate species in the atmospheric degradation of many volatile organic compounds (VOCs) in the troposphere[1] and is commonly found in air, water, and industrial products. The unimolecular tautomerization of gaseous ethenol to ethanal and hydroxyethylidene, $CH_2{=}CH{-}OH \leftrightarrow CH_3CH{=}O \leftrightarrow CH_3{-}C{-}OH$, has been the subject of numerous theoretical and experimental investigations.[2−8] In early reports,[9−24] the $[C_2H_4O]^{\bullet+}$ system was described and calculated that no fewer than 11 isomers exist on potential energy surface.

Various theoretical studies were devoted to the keto−enol tautomerism of $[C_2H_4O]^{\bullet+}$ radical cations.[25−28] The common conclusion of these studies was that in complete agreement with experimental results ab initio molecular orbital calculations predict that ionized hydroxycarbene, $[CH_3COH]^{\bullet+}$, does not only exist as a stable $C_2H_4O^{\bullet+}$ isomer, but also serves as the key intermediate during dissociation of ionized vinyl alcohol ($[CH_2{=}CHOH]^{\bullet+}$) and its isomerization to acetaldehyde ($[CH_3CHO]^{\bullet+}$). Yadav and Goddard[29] examined the isomerization of CH_3CHO to CH_3COH and CH_3OCH, and found the energy barriers to be ∼90 kcal/mol for CH_3COH and ∼100 kcal/mol for CH_3OCH. A similar result may be reached by examining the G1 level of Smith et al.[30] Recently, proton transport that would interconvert the C_2H_4O keto−enol isomers and the corresponding radical cations were characterized in experiments[31] and theory.[32]

The unimolecular decomposition of acetaldehyde was also studied extensively. Yadav and Goddard[33] investigated the radical and molecular dissociation of CH_3CHO using SCF calculations and reported the C−C bond energy in CH_3CHO to be 76 kcal/mol, while molecular decomposition of CH_3CHO to CH_4 and CO requires 84 kcal/mol activation energy. Other studies support the lower activation energy value, e.g., 83 kcal/mol by G2 and 81 kcal/mol at the B3LYP/cc-pVTZ(-f) level of theory for the latter case.[34,35] In addition, there have been extensive experimental and theoretical studies for the potential energy surfaces and the unimolecular dissociation reaction of ethylene oxide (*c*-C_2H_4O, oxirane) as well as ring-opened oxirane.[36−40] Major products observed include ethane, ethylene, methane, acetylene, acetaldehyde, propane, hydrogen, methyl, formyl radical, and so on. These fragment products are of fundamental importance because these molecules exist ubiquitously not only in the atmosphere but also in interstellar molecular clouds, which of them are indicative in elucidating the origin of life, such as fundamental reactions of carbon monoxide and methane, bridging small inorganic molecules to complicated organic functional groups. Furthermore, industrially, the reaction between acetylene and water, $C_2H_2 + H_2O = CH_2{-}CO + H_2$, turning H_2O into H_2, can form so-called water-gas shift for efficient fuel energy production.

On the other hand, the potential energy surface of the electrophilic addition reaction of the oxygen atom O (^3P) with the simplest alkene, C_2H_4 (X^1A_g), which plays an important role in the C_2H_4/O_2 flames and in hydrocarbon combustion in general, was theoretically reinvestigated using various quantum chemical methods, including G3, CBS-QB3, G2M (CC, MP2), and MRCI.[41] Moreover, it is well-known that some reactive fragments, such as CH_3, CHO, H, CH_2CHO, CH_2, H_2CO, $CH_3{-}CO$, H_2CCO, C_2H_2, and so on, are thought to be responsible for photochemical air pollution. These reactions, in which some combinations are all stoichiometrically the same as acetaldehyde (CH_3CHO), are of fundamental importance in chemical kinetics and challenging to theoretical chemists because of their complicated reaction mechanism. However, these reports did not consider the entire system of neutral C_2H_4O isomers, nor did they involve all the relevant intermediates and transition states. Obviously, it is desirable to know how and which stable forms

* Corresponding author. E-mail: ohnok@qpcrkk.chem.tohoku.ac.jp.

10.1021/jp071238d CCC: $37.00
Published on Web 05/17/2007

TABLE 1: Relative Energies (kcal/mol) of Various Singlet [C_2, H_4, O] Isomers and Isomerization Transition States at the DFT/B3LYP/6-311++G(d,p) and Single-Point CCSD(T)/cc-pVTZ//DFT/B3LYP/6-311++G(d,p) Levels with ZPE Correction

species	sym.	ΔZPE B3LYP/6-311++G(d,p)	B3LYP/6-311++G (d,p)+ZPE	CCSD(T)/cc-pVTZ//DFT/ B3LYP/6-311++G(d,p)+ZP E
CH_3CHO (EQ0)[a]	C_1	0.00	0.00	0.00
trans-CH_2CHOH (EQ1a)	C_s	0.69	11.11	10.67
cis-CH_2CHOH (EQ1b)	C_s	0.50	12.24	11.99
c-CH_2OCH_2 (EQ2)	C_{2v}	1.19	30.12	27.86
trans-CH_3COH (IM1a)	C_s	−0.19	50.83	50.64
cis-CH_3COH (IM1b)	C_s	−0.75	54.03	53.34
trans-CH_3OCH (IM2a)	C_s	−0.25	68.02	67.21
cis-CH_3OCH (IM2b)	C_s	−0.69	72.29	70.66
CH_2OCH_2 (IM3)	C_{2v}	−1.07	72.10	72.79
trans-$CHCH_2OH$ (IM4a)	C_1	−0.38	95.69	93.31
cis-$CHCH_2OH$ (IM4b)	C_1	−0.69	99.58	96.82
trans-$HCOHCH_2$ (IM5a)	C_s	−0.56	160.64	160.33
trans-$HCOHCH_2$ (IM5b)	C_1	−0.59	159.70	160.64
cis-$HCOHCH_2$ (IM5c)	C_1	−0.64	164.78	166.41
TS_0/0 (1)*[b]	C_1	−0.19	0.88	0.94
TS_1a/1b	C_1	−0.06	15.56	14.87
TS_C1a/C1a*	C_{2v}	−3.07	35.64	34.89
TS_C1a/C1b	C_s	−3.26	37.88	37.06
TS_IM1a/IM1a*	C_1	−0.38	51.77	51.39
TS_IM1b/IM1b*	C_1	−1.00	55.66	54.47
TS_0/1a	C_s	−3.20	66.33	67.02
TS_IM2a/IM2a*	C_1	−0.44	68.71	67.90
TS_IM2b/IM2b*	C_1	−0.88	72.73	71.10
TS_1a/1a (1)*	C_1	−2.07	70.78	73.35
TS_1b/IM1a	C_1	−2.20	73.17	74.36
TS_IM2a/IM2b (1)	C_1	−5.52	73.39	74.92
TS_IM1a/IM1b (1)	C_1	−2.45	75.30	75.74
TS_C2a/C2a (1)*	C_s	−4.89	76.05	77.06
TS_C2a/C2b	C_s	−4.58	76.74	77.60
TS_C2a/C2a (2)*	C_{2v}	−5.21	77.06	77.68
TS_1a/IM1b	C_1	−2.70	77.43	77.75
TS_C1a/C2a	C_s	−6.28	78.50	77.94
TS_0/IM1a	C_1	−3.64	79.50	79.32
TS_0/2	C_1	−2.95	89.73	81.76
TS_0/0 (2)*	C_1	−3.95	80.45	82.58
TS_0/DC (1)**	C_1	−3.83	80.70	83.02
TS_2/IM3	C_1	−1.63	88.79	83.65
TS_IM1b/DC (1)**	C_1	−5.96	82.64	84.40
TS_1b/1b (1)*	C_1	−2.57	81.64	85.21
TS_1a/1a (2)*	C_1	−2.45	86.16	86.91
TS_1b/1b (2)*	C_1	−2.57	82.96	87.16
TS_IM3/IM3 (1)*	D_{2d}	−1.69	84.27	88.41
TS_1b/1b (3)*	C_1	−2.51	88.60	89.48
TS_1b/C1b (1)	C_1	−3.95	89.11	89.48
TS_IM2b/DC**	C_1	−3.70	99.46	89.86
TS_1a/1a (3)*	C_1	−2.70	89.04	90.11
TS_1b/1b (4)*	C_1	−2.57	90.11	90.17
TS_1a/C2b	C_1	−4.71	89.61	90.92
TS_2/IM4a	C_1	−2.32	99.40	96.20
TS_1b/DC**	C_1	−5.40	94.00	96.51
TS_IM2a/IM2b (2)	C_1	−2.07	97.01	97.14
TS_1a/IM4a (1)	C_1	−1.51	98.20	97.64
TS_1b/IM4a (1)	C_1	−1.51	98.83	97.64
TS_IM3/IM3 (2)*	C_1	−2.13	99.96	99.33
TS_0/DC (2)**	C_1	−7.53	94.88	101.03
TS_2/IM2b	C_1	−2.38	105.23	102.72
TS_0/DC (3)**	C_1	−8.47	102.66	104.10
TS_IM3/IM3 (3)*	C_1	−2.89	107.80	106.30
TS_1b/IM4a (2)	C_s	−1.13	107.68	108.18
TS_1a/IM4a (2)	C_1	−1.13	110.82	110.82
TS_1a/IM4b	C_1	−1.38	111.63	111.13
TS_IM1a/DC (1)**	C_1	−6.09	106.74	111.19
TS_IM3/C3	C_1	−6.28	112.95	111.63
TS_IM1a/C2b	C_1	−4.20	113.08	112.32
TS_1b/IM4b	C_1	−1.69	113.26	113.01
TS_IM2a/IM3	C_1	−4.02	113.45	113.64
TS_IM1b/DC (2)**	C_1	−6.59	110.57	114.02
TS_0/IM2a	C_1	−2.45	113.95	114.08
TS_2/DC (1)**	C_1	−4.96	116.78	115.33
TS_1a/C1b	C_1	−4.71	114.58	118.16
TS_1b/C1b (2)	C_1	−4.77	115.08	119.04
TS_0/DC (4)**	C_1	−4.96	120.42	121.04

TABLE 1: (Continued)

species	sym.	ΔZPE B3LYP/6-311++G(d,p)	B3LYP/6-311++G (d,p)+ZPE	CCSD(T)/cc-pVTZ//DFT/ B3LYP/6-311++G(d,p)+ZP E
TS_1a/DC (1)**	C_1	−6.09	118.85	122.43
TS_IM1a/IM1b (2)	C_1	−2.76	116.09	122.74
TS_1a/IM1a	C_1	−2.45	121.74	124.25
TS_IM1a/DC (2)**	C_1	−5.08	119.98	126.25
TS_1a/DC (2)**	C_1	−5.52	122.49	126.57
TS_1b/IM1b	C_1	−2.95	126.19	127.88
TS_IM1b/DC (3)**	C_1	−5.40	123.87	129.39
TS_0/IM4b	C_1	−4.77	142.13	140.43
TS_1b/1b (5)*	C_1	−6.46	145.73	146.08
TS_2/DC (2)**	C_1	−6.40	149.47	150.22
TS_IM5a/IM5b (1)	C_1	−3.01	161.33	161.39
TS_IM4a/IM5b	C_1	−2.82	161.90	162.02
TS_IM2a/IM5b	C_s	−5.52	162.65	162.15
TS_IM4a/IM5a	C_1	−3.70	164.66	163.15
TS_IM2b/IM4b	C_1	−5.08	167.86	164.91
TS_1b/IM2b	C_1	−5.33	169.24	165.79
TS_IM2a/DC**	C_s	−7.53	173.38	172.19
TS_IM3/IM5b	C_1	−4.96	176.08	173.69
TS_IM3/IM5c	C_1	−4.58	180.97	174.70
TS_IM5a/IM5b (2)	C_s	−0.75	179.65	182.04
TS_IM5c/IM5c*	C_s	−2.32	187.00	189.25

[a] All values are calculated with regard to the isomer EQ0 for which the total energies are −153.829282 and −153.533279 au at the B3LYP/6-311++G(d,p) and single-point CCSD(T)/cc-pVTZ//DFT/B3LYP/6-311++G(d,p) levels, respectively. The ZPE of the EQ0 at B3LYP/6-311++G(d,p) level is 0.052972 au. [b] Self-conversion transition states are symbolized with asterisk (*), while those TSs for dissociation channels are signed with double asterisks (**).

they can convert each other. To clarify these questions, it is of interest to reinvestigate global reaction routes using a more efficient and powerful theoretical techniques.

In this study, a systematic potential energy surface (PES) surveys of the singlet neutral [C_2, H_4, O] system containing the reaction channels leading to the formation of possible products have thus been constructed making use of the scaled hypersphere search (SHS) method[42−44] at highly correlated ab initio coupled-cluster theory, which will be of great assistance in the identification of some new findings. The SHS method can be used to locate all reaction paths resulting in anharmonic downward distortions of the PES. Combining the SHS technique with a downhill-walking algorithm allows a full topographic analysis of the PES to be obtained for any given chemical composition. This approach has been found to lead to an efficient and accurate estimate of new reaction pathways and transition state regions.[45−49] We investigate this system in a wider energy range and included more possible intermediate and transition state species. Our intention is to give a more complete dynamical picture for possible reaction channels so as to interpret or predict the relevant experimental results.

2. Computational Methods

Reaction pathways around the equilibrium structures of acetaldehyde (CH_3CHO) were first searched on the singlet PES at HF/6-31G level of calculations by the SHS method,[42−44] in which harmonic vibrational frequencies at the same level and intrinsic reaction coordinate (IRC) calculations[50−53] were carried out, to check whether the obtained structure is a minimum or a saddle point and to test whether the transition state connects the right isomers or not, respectively.

Structures of all the singlet minima obtained as well as those of the singlet transition states involved in the SHS method were further refined at the DFT/B3LYP/6-311++G(d,p) level of calculation. Vibrational frequency and IRC calculations starting from each TS on B3LYP/6-311++G(d,p) surface were repeated to confirm that the critical points located were either minima or transition states and the connection between equilibrium structures (EQs), respectively. A total of 14 minimum isomers, 5 dissociation complexes and 79 transition states are ultimately located at the B3LYP/6-311++G(d,p) level by geometry optimizations using structures obtained at the low level calculation as initial guesses. To gain reliable relative energies of each stationary point on PES, single-point calculations were performed at the B3LYP/6-311++G(d,p) optimized geometries by employment of the coupled-cluster level of theory, including the single and double excitations with triple contributions (CCSD(T))[54] with the Dunning's correlation consistent basis sets of triple-ζ quality (cc-pVTZ).[55−57] The zero-point vibrational energy (ZPE) at the DFT/B3LYP/6-311++G(d,p) with a scaling factor of 0.96 are also included for energy correction. Basis set superposition errors (BSSE) calculations were carried out for those weakly bound complexes. All calculations (except for the SHS procedures) were implemented using the Gaussian03 program package.[58]

3. Results and Discussion

The present calculations have revealed 14 equilibrium structures, including 4 stable minima and 10 metastable intermediates numbered as EQ*n* and IM*n* following stability order, respectively; 5 weakly bonded complexes denoted as C*i*; and 79 transition states containing interconversion, self-conversion and dissociation processes marked as TS_*n* (or IM*n*, C*i*)/*m* (or IM*m*, C*i*) for connecting directly with EQ*n* (or IM*n*, C*i*) and EQ*m* (or IM*m*, C*i*). Here, EQs mean equilibrium structures that are of saturated valence bond structures. IMs contain carbene frameworks, which cause high reactivity relative to EQs. Complexes C*i* are related to hydrogen bond or van der waals interaction. All of them make up [C_2, H_4, O] isomers.

The corresponding symmetries and relative energies of all the species calculated at the DFT/B3LYP/6-311++G(d,p) and CCSD(T)/cc-pVTZ//B3LYP/6-311++G(d,p) levels are summarized in Tables 1 and 2, while the possible dissociation channels and relative energies of dissociation products are listed in Table 3. For the sake of simplicity and easy discussion, the reaction pathways characterized by CCSD(T)/cc-pVTZ//B3LYP/

TABLE 2: Relative Energies[a] (kcal/mol) of Complexes and Complexation Energies at the DFT/B3LYP/6-311++G(d,p) and Single-Point CCSD(T)/cc-pVTZ//DFT/B3LYP/6-311++G(d,p) Levels with ZPE and BSSE Correction

complexes	sym.	B3LYP/6-311++G (d,p)+ZPE	CCSD(T)/cc-pVTZ//DFT/ B3LYP/6-311++G(d,p)+ZPE	complexation energies[b]
$CHCH\cdots H_2O$ (C1a)	C_{2v}	35.89	35.01	−2.68 (−2.05)
$CHCH\cdots H_2O$ (C1b)	C_s	36.90	36.02	−1.67 (−1.04)
$CH_2C\cdots H_2O$ (C2a)	C_s	75.99	76.93	−2.96 (−3.02)
$CH_2C\cdots H_2O$ (C2b)	C_s	77.31	77.54	−2.35 (−1.70)
$HCHO\cdots CH_2$ (C3)	C_s	112.86	111.63	−0.93 (−1.39)

[a] Relative energies of all complexes are referred to the singlet global minimum EQ0, for which the total energies are −153.829282 and −153.533279 au at the B3LYP/6-311++G(d,p) and single-point CCSD(T)/cc-pVTZ//DFT/B3LYP/6-311++G(d,p) levels, respectively. The ZPE of the EQ0 at B3LYP/6-311++G(d,p) level is 0.052972 au. [b] Complexation energies are calculated as the energy difference between the energy of complex and the total energies of separate monomers at CCSD(T)/cc-pVTZ//DFT/B3LYP/6-311++G(d,p) Level with ZPE and BSSE correction. The value in the parentheses is calculated at the B3LYP/6-311++G(d,p) level.

TABLE 3: Relative Energies (kcal/mol) of the Dissociation Products of [C_2, H_4, O] Isomers and Energy Barriers for the Possible Dissociation Channels at the DFT/B3LYP/6-311++G(d,p) and Single-Point CCSD(T)/cc-pVTZ//DFT/B3LYP/6-311++G(d,p) Levels with ZPE Correction[a]

	relative energy of products		dissociation energy barrier	
dissociation channel (DC)//dissociation transition state[b]	B3LYP/ 6-311++G(d,p)	CCSD(T)/ cc-pVTZ//DFT	B3LYP/ 6-311++G(d,p)	CCSD(T)/ cc-pVTZ//DFT
CH_3CHO (EQ0) → CH_4 ($^1A_1$) + CO ($^1\Sigma^+$)//TS_0/DC(1)	−35.89	−39.91	80.70	83.02
CH_3CHO (EQ0) → CH_2CO ($^1A_1$) + H_2 ($^1\Sigma_g^+$)//TS_0/DC(2)	−3.45	−5.00	94.88	101.03
CH_3CHO (EQ0) → CHCHO ($^1A'$) + H_2 ($^1\Sigma_g^+$)//TS_0/DC(3)	72.16	72.41	102.66	104.10
CH_3CHO (EQ0) → CH_4 ($^1A_1$) + CO ($^1\Sigma^+$)//TS_0/DC(4)	−35.89	−39.91	120.42	121.04
trans-CH_2CHOH (EQ1a) → HCCOH ($^1A'$) + H_2 ($^1\Sigma_g^+$)//TS_1a/DC(1)	28.80	28.93	107.74	111.76
trans-CH_2CHOH (EQ1a) → HCCOH ($^1A'$) + H_2 ($^1\Sigma_g^+$)//TS_1a/DC(2)	28.80	28.93	111.38	115.90
cis-CH_2CHOH (EQ1b) → CH_2CO ($^1A_1$) + H_2 ($^1\Sigma_g^+$)//TS_1b/DC	−3.45	−5.00	81.76	84.52
c-CH_2OCH_2 (EQ2) → c-CH_2OC ($^1A'$) + H_2 ($^1\Sigma_g^+$)//TS_2/DC(1)	58.36	54.90	86.66	87.47
c-CH_2OCH_2 (EQ2) → CHCHO ($^1A'$) + H_2 ($^1\Sigma_g^+$)//TS_2/DC(2)	72.16	72.41	119.35	122.36
trans-CH_3COH (IM1a) → HCCOH ($^1A'$) + H_2 ($^1\Sigma_g^+$)//TS_IM1a/DC(1)	28.80	28.93	55.91	60.55
trans-CH_3COH (IM1a) → HCCOH ($^1A'$) + H_2 ($^1\Sigma_g^+$)//TS_IM1a/DC(2)	28.80	28.93	69.15	75.61
cis-CH_3COH (IM1b) → CH_2CO ($^1A_1$) + H_2 ($^1\Sigma_g^+$)//TS_IM1b/DC(1)	−3.45	−5.00	28.61	31.06
cis-CH_3COH (IM1b) → HCCOH ($^1A'$) + H_2 ($^1\Sigma_g^+$)//TS_IM1b/DC(2)	28.80	28.93	56.54	60.68
cis-CH_3COH (IM1b) → HCCOH ($^1A'$) + H_2 ($^1\Sigma_g^+$)//TS_IM1b/DC(3)	28.80	28.93	69.84	76.05
trans-CH_3OCH (IM2a) → c-CHOCH ($^1A'$) + H_2 ($^1\Sigma_g^+$)//TS_IM2a/DC	58.36	54.90	105.36	104.98
cis-CH_3OCH (IM2b) → CH_4 ($^1A_1$) + CO ($^1\Sigma^+$)//TS_IM2b/DC	−35.89	−39.91	27.17	19.20

[a] The total energies of the reference isomer EQ0 at the DFT/B3LYP/6-311++G(d,p) and single-point CCSD(T)/cc-pVTZ//DFT/B3LYP/6-311++G(d,p) levels as well as the ZPE at the DFT/B3LYP/6-311++G(d,p) level are listed in footnote *a* of Table 1. [b] The geometries of dissociated transition states TS_*n*/DC(*i*) are shown in Figure 6.

6-311++G(d,p) calculation are shown in Figures 1 and 2, in which possible immediate paths are identified and only the channels of the intermediates on energetically favored paths are pursued further. Figures 3, 4 and 5 depict schematic energetic profiles of the singlet PES for the isomerization among stable C_2H_4O isomers and recombination dissociation channels of C_2H_4O, respectively. Figure 6 shows geometries of direct decomposition transition states of unimolecular C_2H_4O isomers. All geometries and relative energies of transition states are listed in the Supporting Information.

3.1. Equilibrium Structures (EQs) and Complexes of C_2H_4O System. On the singlet C_2H_4O PES, 8 acyclic isomers, one monocyclic structure (EQ2), two quasi-cyclic isomers (IM4a/4b), and three oxygen-based ylides (IM5a/5b/5c) were located as minima, while five weekly bonded complexes were found at CCSD(T)/cc-pVTZ//B3LYP/6-311++G** level, as shown in Figures 1 and 2. The classical aldehyde isomer, i.e., acetaldehyde (EQ0), is identified as the global minimum followed by two competitive vinyl alcohols (EQ1a and EQ1b) with C_s symmetry. The energy differences of 10.67−11.99 kcal/mol (around 44.62−50.12 kJ/mol) between EQ0 and EQ1, which represents the prototypical keto−enol pair, are in good agreement with the previous calculation value of 47 kJ/mol[30] and the experimental value of 41 ± 8 kJ/mol.[16] The rotational energy difference of oxygen-hydrogen bond for EQ1a and EQ1b is calculated as 1.32 kcal/mol. The structure EQ1a with two hydrogen atoms located at the reverse direction of C−O bond is more stable than EQ1b in which hydrogen atoms bonded at C−O lie in the same direction. The fourth lowest-lying stationary point EQ2 with C_{2v} symmetry, namely oxirane with an oxygen-bridged bond (i.e., the ring-closed form of ethylene oxide), is predicted to lie 27.86 kcal/mol above the ground state of acetaldehyde, in excellent agreement with previous thermochemical calculations (27.3 kcal/mol)[59,60] and ab initio calculations including electron correlation (29.3 kcal/mol).[39] It is obvious that an accuracy of the present calculation can be confirmed.

In the present calculations for singlet C_2H_4O system, ten chemically bonded intermediate chain-structures with reactive carbene atoms have been characterized. These are IM1a/IM1b, IM2a/IM2b, IM3, IM4a/IM4b, and IM5a/IM5b/IM5c, as shown in Figures 1 and 2. IM*n*a and IM*n*b/c (n = 1, 2, 4, 5) have the same atomic arrangement, but apparent structural differences being rotational position of hydrogen atom at terminal. It can be found that the isomers with hydrogen and methyl group linked on the opposite side of C−O bond are favorable relative to those on the identical side; e.g., IM1a and IM2a lie below IM1b and IM2b by about 2.70 and 3.45 kcal/mol, respectively. The situation is similar for IM4a and IM4b, in which the energy of IM4a with terminal hydrogens on the counter side is

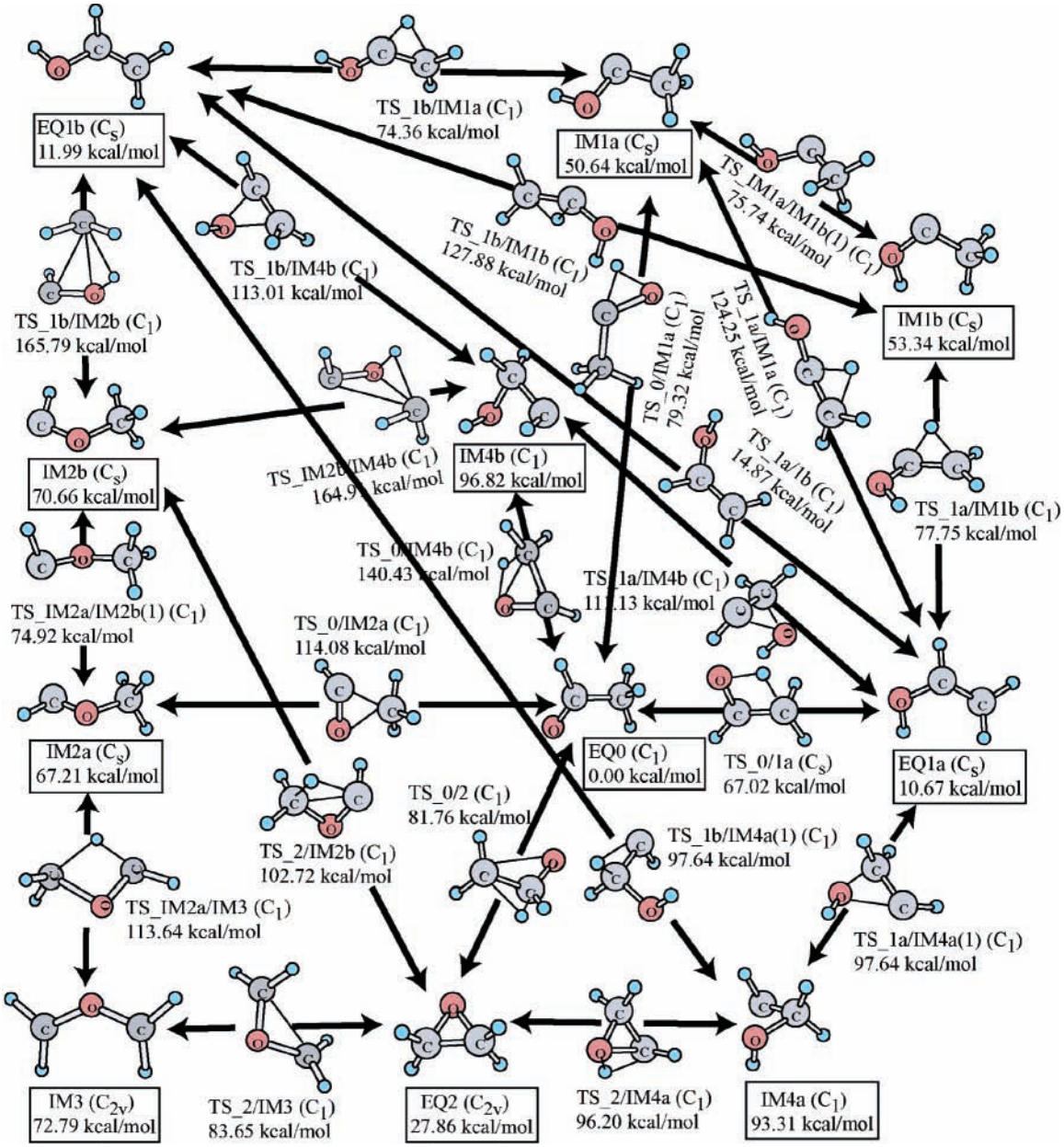

Figure 1. Topology of the unimolecular isomerization pathways for singlet C_2H_4O isomers at the CCSD(T)/cc-pVTZ//B3LYP/6-311++G(d,p) level.

3.51 kcal/mol lower than IM4b with those on the same side. *cis*-IM5 (IM5c) is around 6 kcal/mol higher than *trans*-IM5 (IM5a/5b) as well. The stability of IM*n*a with respect to IM*n*b is possibly due to the fact that the intramolecular steric hindrance is smaller in these structures. From Table 1, one can see that the stability of isomers in which carbene is located in the middle of molecular skeleton is higher as compared with those possessing terminal carbene (relative energies are 50.64−53.34 kcal/mol for IM1 and 67.21−96.82 kcal/mol for IM*n*, $n = 2, 3, 4$). In addition, conformations with carbene atom separated from oxygen by sp^3-hybridized carbon atom (IM4) are thermodynamically unstable relative to those with carbene bonded to oxygen (IM*n*, $n = 1, 2, 3$) because of less electron delocalization in IM4 framework.

One of the ring-opened forms of oxirane, IM3 with C_{2v} symmetry, are predicted to considerably less stable with respect to the ring-closed form EQ2 (44.93 kcal/mol above EQ2), which is consistent with the previous estimates.[39] The other ring-opened form of ethylene oxide, CH_2CH_2O, is observed and suggested to prefer triplet to singlet.[39,41] A similar conclusion may be reached by the present SHS method, in which singlet CH_2CH_2O has not been found as a minimum on the singlet potential energy surface of C_2H_4O at CCSD/cc-pVTZ//B3LYP/6-311++G(d,p) level. It is worthy of note that energy differences between IM2a, IM2b and IM3 are calculated to be 2.13−5.58 kcal/mol, indicating the possibility of a composite metastable peak in metastable state mass spectra analysis arising from a mixture of CH_3OCH and CH_2OCH_2. It is in agreement with neutralization-reionization experiments.[24] Our estimate on the relative energy of hydroxyethylidene (IM1) (212 and 223 kJ/mol for IM1a and IM1b, respectively) is in line with the previous assessments at MP4, QCISD(T), and G1 levels (213∼226 kJ/mol)[30] and the experimental value of 227 ± 8 kJ/mol[61] very well. IM5a/5b/5c are high-energy oxygen-based ylides, which are newly predicted in this report.

Although there have been a few previous ab initio studies of various aspects of the potential energy surface connecting the neutral C_2H_4O isomers,[30,39−41] no more specific complexes

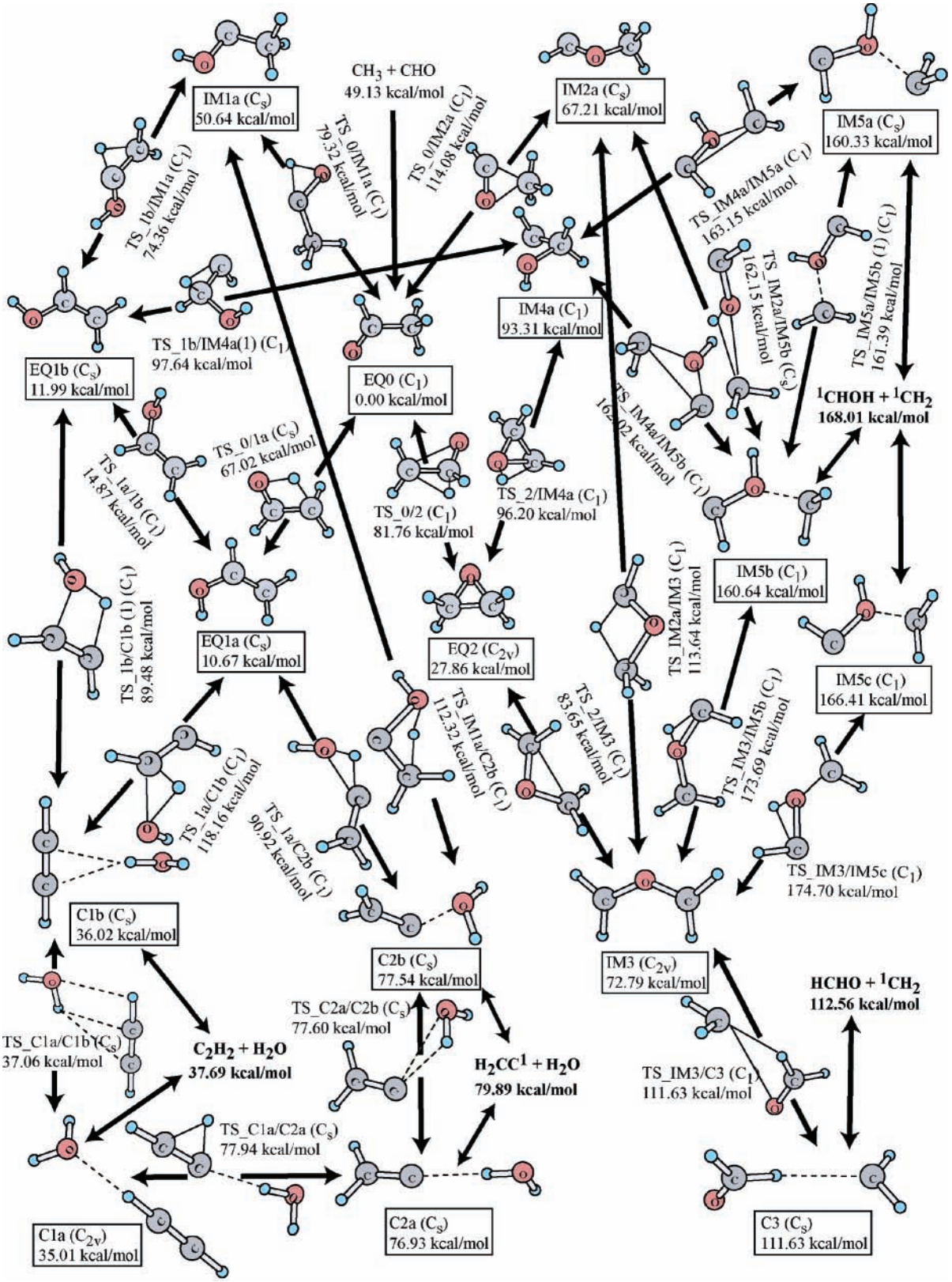

Figure 2. Topology of recombination and dissociation processes for singlet C_2H_4O isomers via intermediates and complexes at the CCSD(T)/cc-pVTZ//B3LYP/6-311++G(d,p) level.

concerning with this system have been investigated. The SHS method presented five weakly bonded complexes made up of stable small molecules or reactive radicals and new transition states involving all relevant rearrangement processes, showing the expected improvements compared with previously reported results. Inspection of the complexation energies reported in Table 2 shows a small amount of the total interaction energy in all cases at CCSD(T)/cc-pVTZ//DFT/B3LYP/6-311++G(d,p) level with ZPE and BSSE corrections. It can be seen that the discovered complex consisted of stable small molecules maintains relatively thermodynamic stability, such as C1a/1b made up of acetylene and water. The remaining complexes are

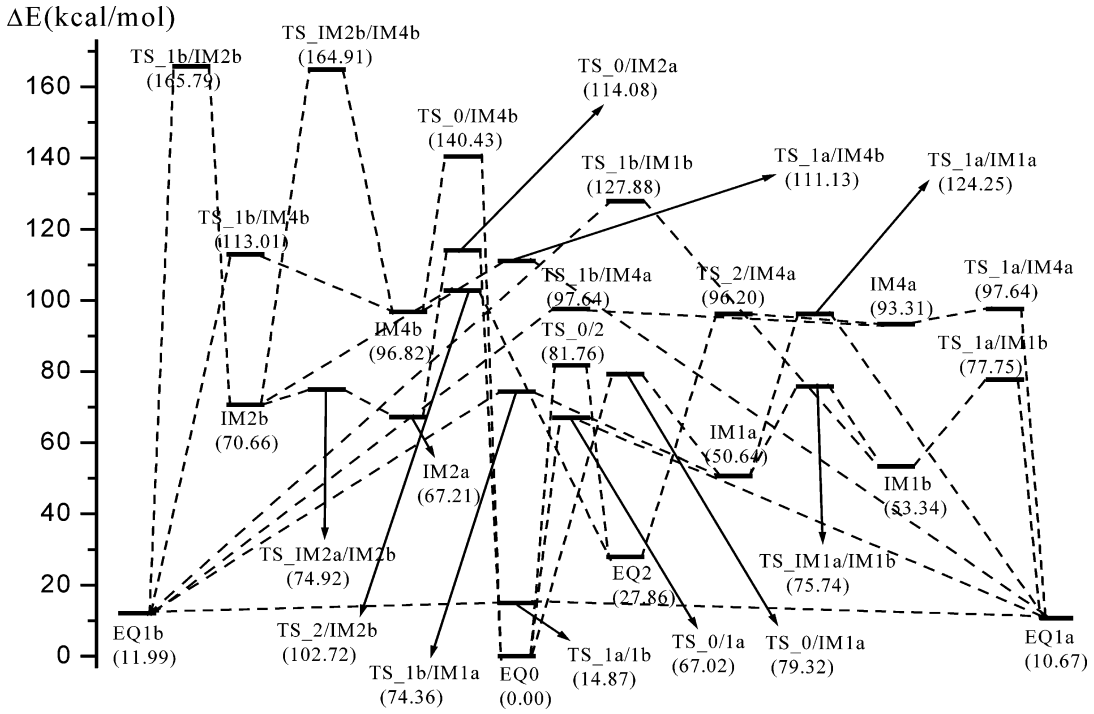

Figure 3. Energetic profile (in kcal/mol) of the potential energy surface for unimolecular isomerization pathways of singlet C_2H_4O isomers at the CCSD(T)/cc-pVTZ//B3LYP/6-311++G(d,p) level.

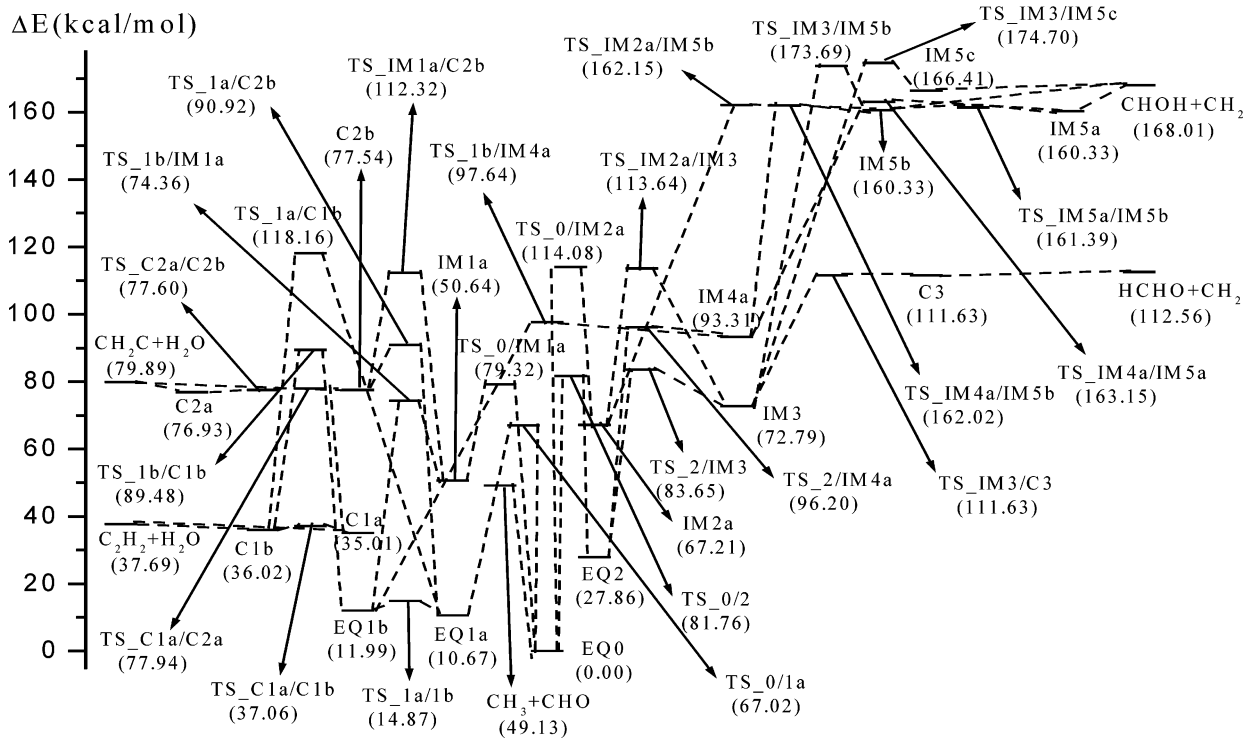

Figure 4. Energetic profile (in kcal/mol) of the potential energy surface for dissociation or recombination channels of singlet C_2H_4O isomers via intermediates and complexes at the CCSD(T)/cc-pVTZ//B3LYP/6-311++G(d,p) level.

combined with distinct components related to sp^3 or sp^2 hybrided carbene. C2a/2b are composed of singlet vinylene and water. C3 is a complex of formaldehyde and methlyene. These complexes are directly associated with the hydrogen bond (HB) interaction except for C2b.

The formation and strengthening of the X−H···Y HB is accompanied by an elongation of the X−H distance in the H-donor monomer whose magnitude usually correlates well with the strength of the interaction, which is a well-known HB effect. Using NBO analysis, it can be indicated that the XH bond length in the XH···Y (Y = oxygen or carbene in our studies) complexes is controlled by a balance between two main factors acting in opposite directions: the hyperconjugative interaction from the lone pair of oxygen or carbene to the σ^* (X−H) antibonding orbital, i.e., n→σ^* interaction, leading to a lengthening of the X−H bond; and the increase of the *s* character and polarization of the XH bond, which could result in a shortening of the X−H distance. In complexes investigated in this work, the first effect is dominant. In addition, stronger HB effect tends to relatively high absolute value of complexation

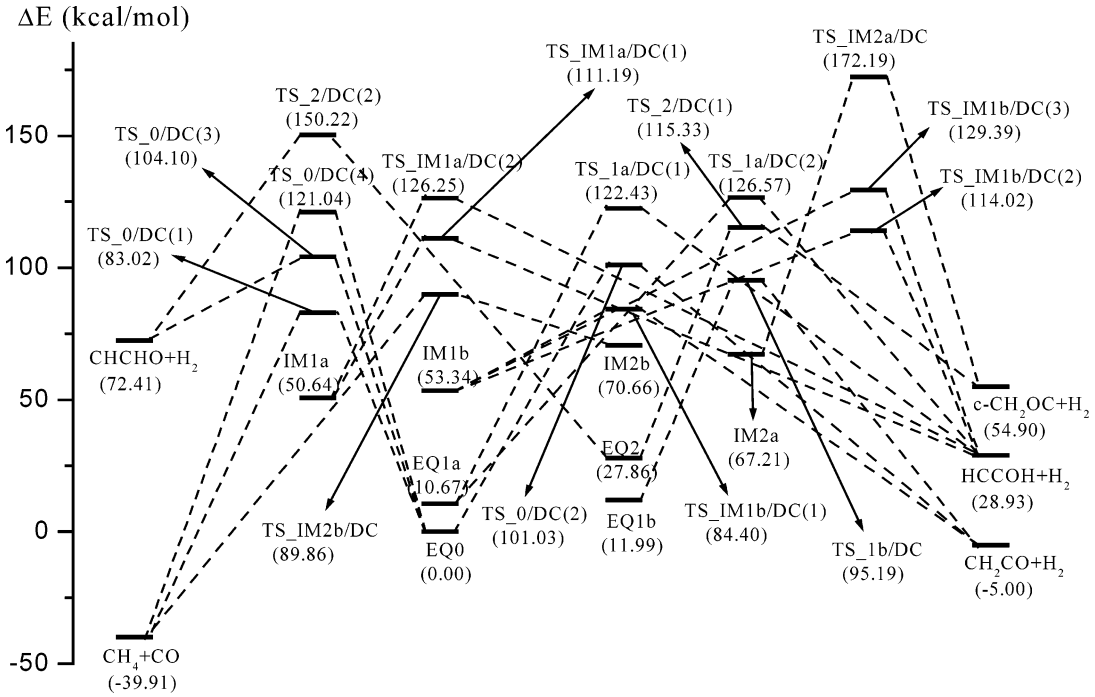

Figure 5. Energetic profile (in kcal/mol) of the potential energy surface for direct decomposition of unimolecular C_2H_4O isomers at the CCSD-(T)/cc-pVTZ//B3LYP/6-311++G(d,p) level.

energy, suggesting the stability of HB complexes is larger with reference to dissociative monomers.

As shown in Figure 2, the thermodynamically stable complexation (C1a) is the σ-cluster of acetylene and water with C_{2v} symmetry, in which the acetylene as an HB donor and the water as an HB acceptor form a straight line of the CHO bond with an H···O HB distance of 2.170 Å. It is followed by the asymmetric π-cluster of acetylene and water (C1b), in which the water as an HB donor is perpendicular to the acetylene as an HB acceptor to form a T-shaped-like structure. Formation of an HB implies a charge-transfer process from the HB acceptor to the HB donor. C1a presents a charge transfer from water to acetylene molecule (−0.008) because of the oxygen of H_2O offering electrons, while C1b shows a charge transfer from acetylene to water (−0.003) on account of the donation of π-electrons in the acetylene molecule. Another important result of the NBO analysis is that the occupation of the σ^* antibonding orbital of the C−H bond in C1a (0.03) is excessive with respect to that of the O−H bond in C1b (0.02), accounting for relatively strong HB interaction in C1a. It is in agreement with the larger extension for the HB donor HCCH in C1a than that for the HB donor H_2O in C1b. Therefore, HCCH···H_2O complex, which lies 2.68 and 1.67 kcal/mol below HCCH + H_2O for C1a and C1b, respectively, is relatively stable as compared with separate monomer derived from the HB interaction. The energy difference between two complexes (C1a and C1b) is very small (only 1 kcal/mol or so), indicating a facile interconversion.

The complex of C2a is formed in term of the HB interaction in which sp^2 carbene of singlet vinylene is a Lewis donor (i.e., electron donor or HB acceptor), and H_2O is a Lewis acceptor (i.e., electron acceptor or HB donor). C2b is formed by a nonbonding π-donation with a C···O distance of 2.347 Å, in which the hyperconjugative interaction is from the lone pair of oxygen in H_2O molecule to the π^* (C−C) antibonding orbital in the singlet vinylene (i.e., n→π^* interaction), reflecting on an elongation of the C−C bond from 1.291 Å to 1.304 Å. Consequently, it is easy to understand instability of C2b with respect to C2a which are from n→σ^* HB interaction.

3.2. Interconversion Pathways among Unimolecular C_2H_4O Isomers. Figure 1 shows isomerization pathways among stable C_2H_4O systems. The related potential energy diagram is illustrated in Figure 3.

The lowest-lying isomer EQ0, acetaldehyde (CH_3CHO), is also kinetically stable relative to all other equilibrium structures, with the lowest conversion barrier of 67.02 kcal/mol by a 1,3-hydrogen migration from carbon to oxygen atom via TS_0/1a (C_s). The reverse process occurs at an activation energy of 56.35 kcal/mol. The SHS method disclosed five independent isomerization pathways starting from the most stable isomer EQ0 (CH_3-CHO) that directly or indirectly result in the formation of other three stable isomers (EQ1a, EQ1b, and EQ2) and six intermediates (IM1a, IM1b, IM2a, IM2b, IM4a, and IM4b).

Two competitive reaction channels starting from EQ0 come forth in the hydrogen transfer processes. One involves the 1,2-H shift and a ring closure, with a barrier height of 81.76 kcal/mol via TS_0/2, to give a cyclic isomer *c*-CH_2OCH_2 (EQ2) possessing C_{2v} symmetry. The reverse barrier height is calculated as 53.90 kcal/mol. The other is a rearrangement of CH_3CHO to the carbene intermediate *trans*-CH_3COH (IM1a) that occurs by a direct 1,2-hydrogen transfer via TS_0/IM1a. The barrier height is 79.32 kcal/mol, which is lower of only 2.44 kcal/mol than that of EQ0 → EQ2. Reaction processes can further take place following *trans*-CH_3COH (IM1a). Over a conversion barrier of 23.72 kcal/mol, 1,2-hydorgen migration happens from the terminal carbon to the intermediate carbon, as shown by TS_1b/IM1a, resulting in the formation of vinyl alcohols *cis*-CH_2CHOH (EQ1b) and then easier interconversion to its isomer *trans*-CH_2CHOH (EQ1a) with the rotational energy barrier of 2.88 kcal/mol. Also a competitive isomerization can occur due to a conversion barrier of 25.10 kcal/mol from *trans*-CH_3COH (IM1a) to *cis*-CH_3COH (IM1b), which takes place by a hydrogen rotation around the oxygen atom on the hydroxyl. As both the H migration and the hydrogen rotation coexist in this process, *trans*-CH_3COH (IM1a) can convert into the stable isomer EQ1a at a high barrier height of 73.61 kcal/mol. Similar to IM1a, another metastable intermediate IM1b can come into

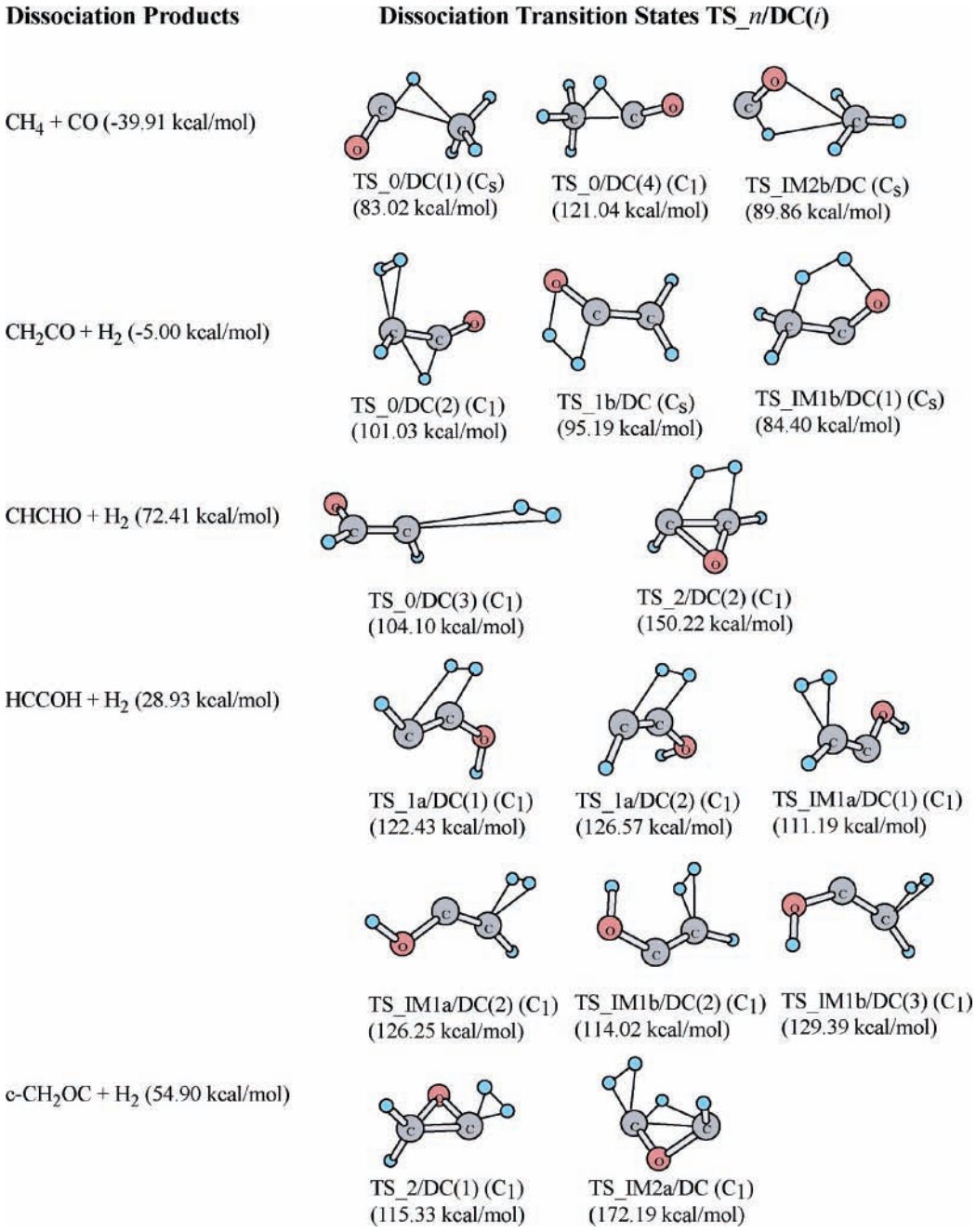

Figure 6. Geometries of direct dissociation transition states of unimolecular C_2H_4O isomers at the CCSD(T)/cc-pVTZ//B3LYP/6-311++G(d,p) level.

being the same stable isomers EQ1a and EQ1b by the H shift or rotation on the different substituent.

Other two reaction pathways starting from EQ0 lie in high-energy transition regions. The high-lying transition states, TS_0/IM2a and TS_0/IM4b (with 114.08 and 140.43 kcal/mol above the global minimum EQ0, respectively), relate to the breaking and recombining of C−C and C−O bond in the EQ0 ↔ IM2a conversion and the twice H shift from the methyl to the CHO in the EQ0 ↔ IM4b process, respectively. Once the metastable carbene intermediates IM2a and IM4b are formed starting from EQ0, they can be exothermic by 55.22 and 84.83 kcal/mol to convert into the stable vinyl alcohol EQ1b, and by 39.35 and 68.96 kcal/mol for the formation of oxirane EQ2 via the identical intermediate *cis*-CH_3OCH (IM2b), respectively. In addition to this, oxirane EQ2 can interconvert with vinyl alcohol (EQ1a and EQ1b) by the two-step mechanism via the unstable intermediate IM4a being of terminal carbene carbon. Both IM4a and IM4b can directly transform to low-lying isomers vinyl alcohol (EQ1a and EQ1b). Although IM4a (*trans*-$CHCH_2OH$) is thermodynamically stable with respect to IM4b (*cis*-$CHCH_2$-OH) (with corresponding relative energies of 93.31 and 96.82 kcal/mol, respectively), it is prone to reside in a very shallow potential well owing to lower barriers of 2.89 (IM4a → EQ2) and 4.33 (IM4a → EQ1a/EQ1b) kcal/mol as compared with that of IM4b (the lowest barrier height is 14.31 kcal/mol at IM4b → EQ1a), indicating its transient nature in kinetics.

3.3. Dissociation or Recombination Processes. Dissociation or recombination processes of C_2H_4O isomers via intermediates and complexes are schematized in Figure 2, while its energetic profile of the potential energy surface is indicated in Figure 4. As shown in Figure 2, there are four entrance channels starting from acetaldehyde to produce complexes or fragments via carbene or ylide intermediates (IM1a, IM2a, IM3, IM4a, and IM5a/5b/5c), once EQ0 is formed by CH_3 + CHO. As

anticipated, no energy barrier is found in these fragment collision processes.

As acetaldehyde (EQ0) is formed through the exothermic combination (an exothermic energy of 49.13 kcal/mol at CCSD-(T) level) between radicals CH_3 and HCO, it could undergo intramolecular rearrangement to produce other single-molecules that further decompose into fragments by way of single or multistep reactions. The following processes including fragmentation could be of interest for combustion and atmospheric relevance. Their pathways are schematically written as follows:

$$\mathrm{EQ0} \rightarrow \mathrm{EQ1a} \rightarrow \mathrm{C1b} \rightarrow \mathrm{C_2H_2} + \mathrm{H_2O} \quad \text{(a)}$$

$$\mathrm{EQ0} \rightarrow \mathrm{EQ1a} \rightarrow \mathrm{C2b} \rightarrow {}^1\mathrm{CH_2C} + \mathrm{H_2O} \quad \text{(b)}$$

$$\mathrm{EQ0} \rightarrow \mathrm{IM1a} \rightarrow \mathrm{EQ1b} \rightarrow \mathrm{C1b} \rightarrow \mathrm{C_2H_2} + \mathrm{H_2O} \quad \text{(c)}$$

$$\mathrm{EQ0} \rightarrow \mathrm{IM1a} \rightarrow \mathrm{C2b} \rightarrow {}^1\mathrm{CH_2C} + \mathrm{H_2O} \quad \text{(d)}$$

$$\mathrm{EQ0} \rightarrow \mathrm{IM2a} \rightarrow \mathrm{IM5b} \rightarrow {}^1\mathrm{CHOH} + {}^1\mathrm{CH_2} \quad \text{(e)}$$

$$\mathrm{EQ0} \rightarrow \mathrm{EQ2} \rightarrow \mathrm{IM4a} \rightarrow \mathrm{IM5a//IM5b} \rightarrow {}^1\mathrm{CHOH} + {}^1\mathrm{CH_2} \quad \text{(f)}$$

$$\mathrm{EQ0} \rightarrow \mathrm{IM2a} \rightarrow \mathrm{IM3} \rightarrow \mathrm{C3//IM5b/5c} \rightarrow \mathrm{H_2CO} + {}^1\mathrm{CH_2//{}^1CHOH} + {}^1\mathrm{CH_2} \quad \text{(g)}$$

$$\mathrm{EQ0} \rightarrow \mathrm{EQ2} \rightarrow \mathrm{IM3} \rightarrow \mathrm{C3//IM5b/5c} \rightarrow \mathrm{H_2CO} + {}^1\mathrm{CH_2//{}^1CHOH} + {}^1\mathrm{CH_2} \quad \text{(h)}$$

As for the former two processes a and b, the rate-determining step should be the direct C−O rupture and hydrogen migration of vinyl alcohol (EQ1a) to produce C1b or C2b, which could further separate into acetylene and water or singlet vinylene and water, respectively. The barrier energies for these two crucial steps are 107.49 (a) and 80.25 kcal/mol (b), indicating the hydrogen shift from carbon connected with oxygen atom to oxygen is preferential in the formation from EQ1a to complexes, i.e., the conversion b is feasible. In reverse, the conversion barriers from complexes to EQ1a imply that the combination of vinyl alcohol and water occur prior to that of acetylene and water, resulting from lower barrier energy by 68.76 kcal/mol. However, as shown in Figure 2, C2b and C2a can interconvert into each other. Particularly, C2b is of transient nature in its kinetic stability in the gas-phase due to a barrier of only 0.06 kcal/mol to form C2a, which could synchronously transform into C1a as a result of the small activation energy of only 1.01 kcal/mol. Sequentially, C1a is apt to disconnect into acetylene and water. In addition, the reverse pathways for this process are unfavorable on account of larger barrier energies relative to respective forward steps, in which reverse barriers are 42.93 and 0.67 kcal/mol for C1a → C2a and C2a → C2b, respectively.

Comparing the first step in all other processes with that in processes a and b, one can notice that the first step in processes a/b is energetically much lower than that in processes c/d, e/g, and f/h by 12.30, 47.06, and 14.74 kcal/mol, respectively. Consequently, it is more necessary to consider the middle and reverse steps for all other processes.

Over a conversion barrier of 23.72 kcal/mol, IM1a can isomerize into stable isomer EQ1b (vinyl alcohol) in process c, which is preferable with regard to its decomposition in process d with a barrier height of 61.68 kcal/mol. The reverse barrier from H_2O + HCCH to IM1a is also higher (34.78 kcal/mol). Apparently, process d is expected to have little contribution. In process c, it can be seen that interconversion between EQ1b and C1b can take place, in which the calculated barrier energies are 77.49 and 53.46 kcal/mol for forward and reverse steps, respectively.

For processes e and f, the forward barriers starting from intermediates IM2a and IM4a to ylides IM5a/5b are 94.94 and 68.71−69.84 kcal/mol, respectively, while reverse barrier heights starting from ylides IM5 to intermediates IM2a and IM4a are only 1.51 and 1.38−2.82 kcal/mol, respectively. In evidence, the reverse routes for processes e and f are predominant. Moreover, IM4a in process f can further isomerize to cyclic isomer EQ2 (oxirane) by the closing of ring and proton transfer with the small activation energy of 2.89 kcal/mol. EQ2 can successively interconverse with EQ0, as mentioned above. Similarly, the forward routes starting from the intermediate IM3 to fragments in processes g and h are unfavorable with respect to the reverse steps. The range of barrier heights is 38.84−101.91 kcal/mol for the forward routes, while only a range of 0.01−13.05 kcal/mol for the reverse steps. Furthermore, IM3 seems to prefer to converse into cyclic isomer EQ2 in process h rather than IM2a in process g arising from the lower activation energy of 10.86 kcal/mol (an activation energy of 40.85 kcal/mol in process g). In summary, the most favorable reaction mechanism between the unimolecular isomers and complexes or dissociated products could be implicated as follows:

path 1: $\mathrm{EQ0} \rightleftharpoons \mathrm{EQ1a} \rightleftharpoons \mathrm{C2b} \rightarrow \mathrm{C2a} \rightarrow \mathrm{C1a} \rightarrow \mathrm{C_2H_2} + \mathrm{H_2O}$

path 2: $\mathrm{EQ1b} \rightleftharpoons \mathrm{C1b} \rightarrow \mathrm{C_2H_2} + \mathrm{H_2O}$

path 3: ${}^1\mathrm{CHOH} + {}^1\mathrm{CH_2} \rightarrow \mathrm{IM5} \begin{Bmatrix} \mathrm{IM5b} \\ \mathrm{IM5a/5b} \end{Bmatrix} \rightarrow \begin{bmatrix} \mathrm{IM2a} \\ \mathrm{IM4a} \rightarrow \mathrm{EQ2} \end{bmatrix} \rightarrow \mathrm{EQ0}$

path 4: $\left.\begin{matrix} \mathrm{H_2CO} + {}^1\mathrm{CH_2} \rightarrow \mathrm{C3} \\ {}^1\mathrm{CHOH} + {}^1\mathrm{CH_2} \rightarrow \mathrm{IM5c} \end{matrix}\right] \rightarrow \mathrm{IM3} \rightarrow \mathrm{EQ2} \rightarrow \mathrm{EQ0}$

At present, there are no reports about these most probable paths, which are actually important not only in the atmosphere but also in interstellar molecular clouds. Especially, the dissociation of vinyl alcohols (EQ1) into acetylene and water (paths 1 and 2), and the formation of ethylene oxide (EQ2) via the reaction between formaldehyde and singlet methylene (path 4) open up a new prediction and picture for the relevant experiment.

3.4. Direct Decomposition of Unimolecular C_2H_4O Isomers. Details of decomposition of single-molecule C_2H_4O isomers inclusive of corresponding transistion states (TS_n/DC(*i*)) are presented in Table 3. The related potential energy diagram is illustrated in Figure 5. The corresponding transition states (TS_*n*/DC(*i*)) are displayed in Figure 6. As can be seen, the most stable unimolecular isomer EQ0 (acetaldehyde) can dissociate into some small molecules which exist ubiquitously not only in the atmosphere but also in interstellar molecular clouds, such as carbon monoxide CO ($^1\Sigma^+$) and methane CH_4 ($^1A_1$), ketene CH_2CO ($^1A_1$) and hydrogen molecule H_2 ($^1\Sigma_g^+$), and CHCHO ($^1A'$) + H_2 ($^1\Sigma_g^+$). The C−C bond rupture in the dissociation channels of EQ0 via TS_0/DC (1) is calculated to be lower in energy than other decomposition processes of EQ0. The dissociation energy barrier is 83.02 kcal/mol at the CCSD-(T)/cc-pVTZ level, while the reverse barrier is 122.93 kcal/mol. This activation energy is in complete agreement with the previous reports.[33−35] The reaction of H_2 addition to HCCHO

is relatively favorable to form EQ0 with respect to H_2 elimination from EQ0, in which barrier heights are 31.69 and 104.10 kcal/mol, respectively.

Raising vinyl alcohol's energy to a higher level, the hydrogen abstraction can occur to form ethynyl alcohol and ketene for trans and cis geometries via TS_1a/DC and TS_1b/DC, respectively. The barrier heights are over 84 kcal/mol, while the reverse association processes are similarly energy demanding (with barrier heights of more than 93 kcal/mol). Over dissociation energy of 87.47 kcal/mol, cyclic isomer oxirane (EQ2) can abstract two hydrogen atoms from a carbon atom as a result of strong CH_2 rocking modes, leading to the formation of H_2 and *c*-CH_2OC with C_s symmetry. Another dissociation channel of EQ2 is the formation of CHCHO ($^1A'$) + H_2 ($^1\Sigma_g^+$), which is of higher activation energies for the forward and reverse processes compared with similar decomposition of EQ0 (CH_3-CHO (EQ0) $\rightarrow$ CHCHO ($^1A'$) + H_2 ($^1\Sigma_g^+$)).

With reference to the stable isomer, the decomposition of metastable intermediates is feasible owing to the lone electron pair on the carbene carbon. The H_2 elimination resulting in the formation of ethynyl alcohol in IM1a (*trans*-CH_3COH) and IM1b (*cis*-CH_3COH) are competitive, possessing the dissociation barrier of around 60 kcal/mol. However, 1,3-hydrogen abstraction in IM1b (*cis*-CH_3COH) to produce ketene and hydrogen molecule is preferentially derived from the coupled motion of CCO framework stretching and the least steric hindrance effect. In two dissociation channels of IM2 (IM2a and IM2b), *cis*-CH_3-OCH (IM2b) is apt to break down into carbon monoxide and methane, on account of largely a H_3C-O stretching motion leading to a cleaved C−O bond, which is more energy undemanding than another DC in which a ring-closing COC skeleton is formed. The dissociation energy barriers are 19.20 and 104.98 kcal/mol, respectively.

4. Conclusions

The global analysis of the singlet potential energy surface for neutral acetaldehyde (CH_3CHO), including 79 transition states, 14 equilibrium structures, 5 complexes as well as 21 dissociation or recombination channels, can be discovered by the SHS method at the CCSD(T)/cc-pVTZ//DFT/B3LYP/6-311++G(d,p) level. Our calculations disclosed three oxygen-based ylides (IM5a/5b/5c), while the remaining eleven isomers in C_2H_4O system are in accord with the previous reports.[16,30,39−41,59,60] Those stable isomers EQ*n* (n = 0−2) with thermodynamic stability are also found to be kinetically stable with reference to metastable intermediates IM*n*. In addition, the position of carbene carbon in molecule plays a key role in stability for intermediates, in which those with carbene located in the middle of molecular skeleton are more stable as compared with those possessing terminal carbene.

Possible routes for interconversion and dissociation have been revealed that radiation may isomerize or dissociate the initial singlet acetaldehyde into energetically more favorable channels so as to rearrange to other isomers or small molecules. The decomposition pathways of various isomers conversely provide the recombination possibility from simple fragments detected in combustion or interstellar space. The results of the current investigation establish a detailed picture of the products and metastable intermediates, identifies the paths below the energy of the separated reactants, and predicts the most likely products. Most transition states and reaction pathways for the neutral CH_3-CHO are discovered for the first time, which should be helpful to be incorporated in future chemical models of interstellar clouds.

Acknowledgment. This work was supported by a Grant-in-Aid for Scientific Research from the Japanese Ministry of Education, Culture, Sports, Science, and Technology. X.Y. is supported by the Research Fellowship of the Japan Society for the Promotion of Science for a JSPS postdoctoral fellowship (ID: P06063). S.M. is supported by the Research Fellowship of the Japan Society for the Promotion of Science for Young Scientists.

Supporting Information Available: List of transition states and relative energies. This material is available free of charge via the Internet at http://pubs.acs.org.

References and Notes

(1) Atkinson, R.; Arey, J. *Chem. Rev.* **2003**, *103*, 4605.
(2) Bouma, W. J.; Poppinger, D.; Radom, L. *J. Am. Chem. Soc.* **1977**, *99*, 6443.
(3) Bouma, W. J.; Vincent, M. A.; Radom, L. *Int. J. Quantum Chem.* **1978**, *14*, 767.
(4) Rodwell, W. R.; Bouma, W. J.; Radom, L. *Int. J. Quantum Chem.* **1980**, *18*, 107.
(5) Nobes, R. H.; Radom, L.; Alinger, N. L. *J. Mol. Struct.* **1981**, *85*, 185.
(6) Splitter, J. S.; Calvin, M. *J. Am. Chem. Soc.* **1979**, *101*, 7329.
(7) Faustov, V. I. F.; Yufit, S. S. *Zh. Fiz. Khim.* **1982**, *56*, 2226.
(8) Wesdemiotis, C.; McLafferty, F. W. *J. Am. Chem. Soc.* **1987**, *109*, 4760.
(9) Van de Sande, C. C.; McLafferty, F. W. *J. Am. Chem. Soc.* **1975**, *97*, 4613.
(10) Corderman, R. R.; LeBretan, P. R.; Butrill, S. E., Jr.; Williamson, A. D.; Beauchamp, J. L. *J. Chem. Phys.* **1976**, *65*, 4929.
(11) Holmes, J. L.; Terlouw, J. K.; Lossing, F. P. *J. Phys. Chem.* **1976**, *80*, 2860.
(12) Kumakura, M.; Arakawa, K.; Sugiura, T. *Int. J. Mass. Spectrom. Ion. Phys.* **1978**, *26*, 303.
(13) Bouma, W. J.; MacLeod, J. K.; Radom, L. *Adv. Mass. Spectrom.* **1979**, *8A*, 178.
(14) Bouma, W. J.; MacLeod, J. K.; Radom, L. *J. Am. Chem. Soc.* **1979**, *101*, 5540.
(15) Baumann, B. C.; MacLeod, J. K. *J. Am. Chem. Soc.* **1981**, *103*, 6223.
(16) Holmes, J. L.; Lossing, F. P. *J. Am. Chem. Soc.* **1982**, *104*, 2648.
(17) Protor, C. J.; McLafferty, F. W. *Org. Mass. Spectrom.* **1983**, *18*, 193.
(18) Terlouw, J. K.; Wezenberg, J.; Burgers, P. C.; Holmes, J. L. *J. Chem. Soc., Chem. Commun.* 1**983**, 1121.
(19) Turecek, F.; Hanus, V. *Org. Mass Spectrom.* **1984**, *19*, 423.
(20) Burgers, P. C.; Terlouw, J. K.; Holmes, J. L. *Int. J. Mass. Spectrom. Ion. proc.* **1985**, *65*, 91.
(21) Iraqui, M.; Pri-Bar, I.; Lifshitz, C. *Org. Mass Spectrom.* **1986**, *21*, 661.
(22) Buschek, J. M.; Holmes, J. L.; Terlouw, J. K. *J. Am. Chem. Soc.* **1987**, *109*, 7321.
(23) Mabud, Md. A.; Ast, T.; Verma, S.; Jiang, Y.-X.; Cooks, R. G. *J. Am. Chem. Soc.* **1987**, *109*, 7597.
(24) Wesdemiotis, C.; Leyh, B.; Fura, A.; McLafferty, F. W. *J. Am. Chem. Soc.* **1990**, *112*, 8655.
(25) Apeloig, Y.; Karni, M.; Ciommer, B.; Depke, G.; Frenking, G.; Meyn, S.; Schmidt, J.; Schwarz, H. *J. Chem. Soc., Chem. Commun.* **1983**, 1497.
(26) Apeloig, Y.; Karni, M.; Ciommer, B.; Depke, G.; Frenking, G.; Meyr, S.; Schmidt, J.; Schwarz, H. *J. Chem. Soc., Chem. Commun.* 1**984**, *57*, 179.
(27) Apeloig, Y.; Karni, M.; Ciommer, B.; Depke, G.; Frenking, G.; Meyn, S.; Schmidt, J.; Schwarz, H. *Int. J. Mass. Spectrom. Ion. Processes* **1984**, *59*, 21.
(28) Bertrand, W.; Bouchoux, G. *Rapid Commun. Mass Spectrom.* **1998**, *12*, 1697.
(29) Yadav, J. S.; Goddard, J. D. *J. Chem. Phys.* **1986**, *85*, 3975.
(30) Smith, B. J.; Nguyen, M. T.; Bouma, W. J.; Radom, L. *J. Am. Chem. Soc.* **1991**, *113*, 6452.
(31) Van der Rest, G.; Nedev, H.; Chamot-Rooke, J.; Mourgues, P.; McMahon, T. B.; Audier, H. E. *Int. J. Mass Spectrom.* **2000**, *202*, 161.
(32) Hudson, C. E.; McAdoo, D. J. *Int. J. Mass Spectrom.* **2002**, *219*, 295.
(33) Yadav, J. S.; Goddard, J. D. *J. Chem. Phys.* **1986**, *84*, 2682.
(34) Martell, J. M.; Yu, H.; Goddard, J. D. *Mol. Phys.* **1997**, *92*, 497.
(35) Gherman, B. F.; Friesner, R. A.; Wong, T.-H.; Min, Z.; Bersohn, R. *J. Chem. Phys.* **2001**, *114*, 6128.

(36) Benson, S. W. *J. Chem. Phys.* **1964**, *40*, 105.
(37) Setser, D. W. *J. Phys. Chem.* **1966**, *70*, 826.
(38) Lifshitz, A.; Ben-Hamou, H. *J. Phys. Chem.* **1983**, *87*, 1782.
(39) Belbruno, J. J. *J. Phys. Org. Chem.* **1997**, *10*, 113.
(40) Joshi, A.; You, X.; Barckholtz, T. A.; Wang, H. *J. Phys. Chem. A* **2005**, *109*, 8016.
(41) Nguyen, T. L.; Vereecken, L.; Hou, X. J.; Nguyen, M. T.; Peeters, J. *J. Phys. Chem. A* **2005**, *109*, 7489.
(42) Ohno, K.; Maeda, S. *Chem. Phys. Lett.* **2004**, *384*, 277.
(43) Maeda, S.; Ohno, K. *J. Phys. Chem. A* **2005**, *109*, 5742.
(44) Ohno, K.; Maeda, S. *J. Phys. Chem. A* **2006**, *110*, 8933.
(45) Maeda, S.; Ohno, K. *Chem. Lett.* **2004**, *33*, 1372.
(46) Maeda, S.; Ohno, K. *Chem. Phys. Lett*. **2004**, *398*, 240.
(47) Maeda, S.; Ohno, K. *Chem. Phys. Lett.* **2005**, *95*, 404.
(48) Yang, X.; Maeda, S.; Ohno, K. *J. Phys. Chem. A* **2005**, *109*, 7319.
(49) Yang, X.; Maeda, S.; Ohno, K. *Chem. Phys. Lett.* **2006**, *418*, 208.
(50) Fukui, K. *Acc. Chem. Res.* **1981**, *14*, 363.
(51) Page, M.; Mclver, J. W., Jr. *J. Chem. Phys.* **1988**, *88*, 922.
(52) Gonzalez, C.; Schlegel, H. B. *J. Chem. Phys.* **1989**, *90*, 2154.
(53) Gonzalez, C.; Schlegel, H. B. *J. Chem. Phys.* **1990**, *94*, 5523.
(54) Raghavachari, K.; Trucks, G. W.; Pople, J. A.; Head-Gordon, M. *Chem. Phys. Lett.* **1989**, *157*, 479.
(55) Dunning, T. H. *J. Chem. Phys.* **1989**, *90*, 1007.
(56) Kendall. R. A.; Dunning, T. H.; Harrison, R. J. *J. Chem. Phys.* **1992**, *96*, 6796.
(57) Woon, D. E.; Dunning, T. H. *J. Chem. Phys.* **1993**, *98*, 1358.
(58) Frisch, M. J.; Trucks, G. W.; Schlegel, H. B.; Scuseria, G. E.; Robb, M. A.; Cheeseman, J. R.; Montgomery, J. A., Jr.; Vreven, T.; Kudin, K. N.; Burant, J. C.; Millam, J. M.; Iyengar, S. S.; Tomasi, J.; Barone, V.; Mennucci, B.; Cossi, M.; Scalmani, G.; Rega, N.; Petersson, G. A.; Nakatsuji, H.; Hada, M.; Ehara, M.; Toyota, K.; Fukuda, R.; Hasegawa, J.; Ishida, M.; Nakajima, T.; Honda, Y.; Kitao, O.; Nakai, H.; Klene, M.; Li, X.; Knox, J. E.; Hratchian, H. P.; Cross, J. B.; Adamo, C.; Jaramillo, J.; Gomperts, R.; Stratmann, R. E.; Yazyev, O.; Austin, A. J.; Cammi, R.; Pomelli, C.; Ochterski, J. W.; Ayala, P. Y.; Morokuma, K.; Voth, G. A.; Salvador, P.; Dannenberg, J. J.; Zakrzewski, V. G.; Dapprich, S.; Daniels, A. D.; Strain, M. C.; Farkas, O.; Malick, D. K.; Rabuck, A. D.; Raghavachari, K.; Foresman, J. B.; Ortiz, J. V.; Cui, Q.; Baboul, A. G.; Clifford, S.; Cioslowski, J.; Stefanov, B. B.; Liu, G.; Liashenko, A.; Piskorz, P.; Komaromi, I.; Martin, R. L.; Fox, D. J.; Keith, T.; Al-Laham, M. A.; Peng, C. Y.; Nanayakkara, A.; Challacombe, M.; Gill, P. M. W.; Johnson, B.; Chen, W.; Wong, M. W.; Gonzalez, C.; Pople, J. A. *Gaussian 03*, revision B.05; Gaussian, Inc.: Pittsburgh, PA, 2003.
(59) Cunningham, G. L.; Boyd, A. W.; Myers, R. J.; Gwinn, W. D.; LeVan, W. I. *J. Chem. Phys.* **1951**, *19*, 676.
(60) Hirose, C. *Bull. Chem. Soc. Jpn.* **1974**, *47*, 1311.
(61) Pan, C. F.; Hehre, W. J. *J. Phys. Chem.* **1982**, *86*, 1252.